J|A|C|S
ARTICLES
Published on Web 09/25/2004

Enol−Enamine Tautomerism in Crystals of 1,3-Bis(pyridin-2-yl) Propan-2-one: A Combined Crystallographic and Quantum-Chemical Investigation of the Effect of Packing on Tautomerization Processes

Oded Godsi,[†] Boaz Turner,[†] Kinga Suwinska,*[,‡] Uri Peskin,*[,†,§] and Yoav Eichen*[,†,⊥]

Contribution from the Department of Chemistry, Solid State Institute, and Lise Mitner Center for Computational Quantum Chemistry, Technion − Israel Institute of Technology, Technion City, 32000 Haifa, Israel, and Institute of Physical Chemistry, Polish Academy of Sciences, Kasprzaka 44/52, PL-01 224 Warszawa, Poland

Received June 22, 2004; E-mail: chryoav@tx.technion.ac.il

Abstract: The enolpyridine, **OH**−ketoenamime, **NH** equilibrium in crystals of 1,3-bis(pyridin-2-yl)propan-2-one was studied using temperature-dependent single-crystal X-ray diffraction. The relative population of the different tautomers was found to be sensitive to the temperature in the range of 100−300 K, illustrating the small thermodynamic difference between these two tautomers. This energy resemblance is partially attributed to the molecular packing in the crystal, where the molecules are arranged in the form of dimers. Ab initio electronic energy calculations (HF/6-31G** and MP2/6-31G**) reveal the effect of dimerization in the crystal on the electronic energy levels. Several tautomeric states were identified in the dimer of 1,3-bis(pyridin-2-yl)propan-2-one. A model is proposed in which four of these dimer states are populated in the crystal at ambient temperatures. The crystallographic data were treated according to this four-state dimer model, suggesting that the free energy of the OH−NH dimers is higher than that of the OH−OH dimers by 120 ± 10 cal mol^{-1} and that the NH−NH dimers are yet higher in free energy by 50 ± 10 cal mol^{-1}.

Introduction

Tautomerization and proton-transfer processes draw considerable scientific attention due to their fundamental importance in many chemical and biochemical processes and their role in different reaction mechanisms.[1] Of special interest are systems in which the tautomerization process takes place in hetero-π-conjugated systems. Such systems are usually characterized by rather strong hydrogen bonds, reportedly due to the interplay between H-bond strengthening and increased π-delocalization of the interleaving heterodiene (the RAHB model developed by Gilli et al.).[2] Many of these systems are found to be involved in the formation of biological supramolecular structures through molecular recognition and self-assembly processes.[3]

In recent years, considerable efforts were directed toward the uncovering and understanding of the basic factors that dictate the tautomeric equilibrium at the molecular level.[4] The roles of the electronic and geometric properties as well as the influence of steric factors on the tautomeric equilibrium and proton-transfer rates in many different structures were studied in detail in systems such as ketones, diketones, acids, amides, amines, etc.[5]

In the solid state, specific and nonspecific interactions that a molecule experiences with its neighbors are not time-averaged, unlike processes in the gas phase and in liquids. The different tautomeric states are usually very similar in energy, in many systems, only a few kcal mol^{-1} from one another. It is thus anticipated that interaction with the environment should have a significant effect on the kinetic and thermodynamic properties of such tautomerizing systems.

[†] Department of Chemistry, Technion, Israel Institute of Technology.
[‡] Polish Academy of Sciences.
[§] Lise Mitner Center for Computational Quantum Chemistry, Technion, Israel Institute of Technology.
[⊥] Solid State Institute, Technion, Israel Institute of Technology.

(1) (a) Lanyi, J. K. *J. Biol. Chem.* **1997**, *272*, 31209−31212. (b) Hirst, J.; Duff, J. L. C.; Jameson, G. N. L.; Kemper, M. A.; Burgess, B. K.; Armstrong, F. A. *J. Am. Chem. Soc.* **1998**, *120*, 7085−7094. (c) Mitchell, P. *Nature* **1961**, *191*, 144−148. (d) Williams, R. J. P. *Biochim. Biophys. Acta* **1991**, *1058*, 71. (e) Babcock, G. T.; Wikström, M. *Nature* **1992**, *356*, 301−309.

(2) (a) Bertolasi, V.; Gilli, P.; Ferretti, V.; Gilli, G. *J. Chem. Soc., Perkin Trans. 2* **1997**, *5*, 945−952. (b) Bertolasi, V.; Gilli, P.; Ferretti, V.; Gilli, G. *Chem.-Eur. J.* **1996**, *2*, 925−934. (c) Gilli, P.; Bertolasi, V.; Ferretti, V.; Gilli, G. *J. Am. Chem. Soc.* **1994**, *116*, 909−915. (d) Bertolasi, V.; Ferretti, V.; Gilli, P.; Gilli, G.; Issa, Y.; Sherif, O. *New J. Chem.* **1994**, *18*, 251−261. (e) Bertolasi, V.; Gilli, P.; Ferretti, V.; Gilli, G. *J. Am. Chem. Soc.* **1991**, *113*, 4917−4925. (f) Gilli, G.; Bellucci, F.; Ferretti, V.; Bertolasi, V. *J. Am. Chem. Soc.* **1989**, *111*, 1023−1028.

(3) Hill, J. D.; Mio, J. M.; Prince, R. B.; Hughes, T. S.; Moore, J. S. *Chem. Rev.* **2001**, *101*, 3893−4011.

(4) (a) Rappoport, Z.; Frey, J.; Sigalov, M.; Rochlin, E. *Pure Appl. Chem.* **1997**, *69*, 1933−1940. (b) Rappoport, Z.; Biali, S. E. *Acc. Chem. Res.* **1988**, *21*, 442−449. (c) Carey, E.; Al-Quatami, S.; O'Ferrall, R *Chem. Commun.* **1988**, *16*, 1097−1098. (d) Acton, A.; Allen, A.; Antunes, L.; Fedorov, A.; Najafian, K.; Tidwell, T.; Wagner, B. *J. Am. Chem. Soc.* **2002**, *124*, 13790−13794.

(5) (a) Lei, Y. X.; Casarini, D.; Cerioni, G.; Rappoport, Z. *J. Org. Chem.* **2003**, *68*, 947−959. (b) Lei, Y. X.; Cerioni, G.; Rappoport, Z. *J. Org. Chem.* **2001**, *66*, 8379−8394. (c) Mukhopadhyaya, J. K.; Sklenak, S.; Rappoport, Z. *J. Org. Chem.* **2000**, *65*, 6856−6867. (d) Wagner, P. J.; Park, B.; Sobczak, M.; Frey, J.; Rappoport, Z. *J. Am. Chem. Soc.* **1995**, *117*, 619−629. (e) Eventova, I.; Nadler, E. B.; Rochlin, E.; Frey, J.; Rappoport, Z. *J. Am. Chem. Soc.* **1993**, *115*, 1290−1302. (f) Bertolasi, V.; Pretto, L.; Gilli, P.; Ferretti, V.; Gilli, G. *New J. Chem.* **2002**, *26*, 1559−1566.

Many keto−enol, enol−enamine, and keto−enol−enamine tautomerization reactions have been studied in the solid state in recent years.[6] Nevertheless, the main focus was put on resonance contributions. In most cases, such systems were analyzed on the isolated molecular level, as if they were reacting in the gas phase. Still, the effect of specific supramolecular interactions between the reacting molecule and its neighbors on the reaction thermodynamics and kinetics is of prime interest, mainly due to its biological relevance.

Evidence for such site dependence in tautomerization and other chemical transformations is frequently found in biological systems[7] but can also be found in numerous solid-state systems.[8] In such systems, a slight variation in the environment of the reactants often results in a significant change in activity or in mechanism path selection.[9] Numerous publications[10−12] report on the effect of the site on the determination of the reaction path of a photorearrangement process in crystals of different ketones and in polyenes.[13] In recent publications,[14] we, and others,[15] have studied the tautomerization of 2(2,4-dinitrobenzyl) pyridine derivatives in single crystals and noted the effect of the molecular environment on the kinetics of the process.[16] We have also reported on the effect of the site on the ring closure kinetics in crystals of spiropyrans.[17]

Here, we report on a combined theoretical−experimental study of the ketopyridine−enolpyridine−ketoenamine tautomerization equilibrium that takes place in the crystal of 1,3-bis-(pyridin-2-yl)propan-2-one. The system was studied using temperature-dependent single-crystal X-ray diffraction to determine the relative population of the different tautomers as a function of the temperature. Quantum-chemical (ab initio, HF/6-31G**, and MP2/6-31G**) study of the system reveals the effect of dimerization of the reacting molecules on the tautomerization potential surface and on the keto−enol−enamine equilibrium.

Experimental Section

Materials. 1,3-Bis(pyridin-2-yl)propan-2-one, **1**, was prepared according to a literature procedure.[18] The compound was column chromatographed (dichloromethane:hexane, 3:7) to yield the pure material as pale yellow crystals, mp = 81−82 °C (80−81 °C lit.). HR-MS: calcd. for $[C_{13}H_{12}N_2O]^+$, 212.0949; found for M^+, 212.0991. ^{1}H NMR ($CDCl_3$): keto form, δ = 8.54 (d 2H), 7.60 (t 2H), 7.15 (t 4H), 4.01 (s 4H); ene-X form, δ = 15.04 (s 1H), δ = 8.54 (d 4H), 8.10 (d 1H), 7.60 (t 6H), 7.48 (d 1H), 7.35 (d 2H), 7.15 (t 10H), 6.85 (d 3H), 5.38 (s 1H), 4.01 (s 9H), 3.77 (s 3H). ^{13}C NMR ($CDCl_3$): keto form, δ = 203.9, 154.6, 149.4, 136.4, 124.3, 122.0, 52.1; ene-X form δ = 203.9, 154.6, 149.6, 149.4, 143.3, 136.5, 136.4, 124.3, 122.0, 121.6, 120.8, 117.9, 96.0, 52.1, 45.9.

Single crystals suitable for X-ray crystallography were prepared by slowly evaporating a solution of **1** in ether. This process yields large yellow crystals. All of the temperature-dependent X-ray diffraction experiments were performed on the same single crystal, starting at 100 K. These temperature-dependent X-ray diffraction experiments were repeated on several crystals, producing the same results.

Crystal Data for 1. $C_{13}H_{12}N_2O$, T = 293(2) K, M_r = 212.25, orthorhombic, space group *Pbcn*, a = 11.1892(4), b = 10.7501(4), c = 17.9978(7), V = 2164.8(1) Å^3, Z = 8, ρ_{calc} = 1.298 g cm^{-3}. R = 0.054 for 1257 independent reflections with $I > 2\sigma(I)$, GOF = 0.884.[19]

Apparatus and Experimental Details. X-ray diffraction data for a crystal of dimensions of 0.3 × 0.2 × 0.15 mm were collected at 100-(2), 150(2), 200(2), 250(2), 293(2), 300(2), and 330(2) K on a Kappa CCD diffractometer using Mo Kα radiation (λ = 0.71073 Å). Data collection was performed using φ and ω scans. The data were collected using the "Collect" software[20] and were processed using the "Denzo" and "Scalepak" software.[21] The structures were solved and refined using the SHELXL-97[22] and SHELXS-97[23] programs. All structural analyses and drawings were done using the WinGX[24] software.

The Fourier maps were calculated with the absence of hydrogen atom H1. The disorder of the H1 atom in the two positions (enol-pyridine−ketoenamime) is clearly visible and is clearly temperature dependent. The partial occupancies of the H1 atom were refined by locating the H1 atom in two positions (bound to the oxygen atom and to the nitrogen atom). All hydrogen parameters were refined according to the following assumptions: (1) The sum of the partial occupancy factors in the two positions is always equal to one. (2) The thermal displacement parameters for the two positions are equal.

For comparison, the structural model without disorder was also analyzed. An enol-type structure of the molecule having positional parameters and thermal parameter of H1 was refined. In the resulting structure, the U_{iso} of H1 was approximately 3 times larger than that of any other H-atom in the molecule. At higher temperatures, the O−H bond was elongated with a tendency to place the H1 atom between the nitrogen and oxygen atoms. The later result confirmed that the disordered model is more accurate for this structure.

Calorimetric measurements were performed on a calibrated DSC (Polymer Science Ltd.) machine. Quantum-chemical calculations were performed using the Gaussian 98 RevA.11.3 package.[25]

Results and Discussion

In Solutions. The tautomer map of 1,3-bis(pyridin-2-yl)-propan-2-one, **1**, is composed of three major tautomeric forms:

(6) (a) Gilli, P.; Bertolasi, V.; Pretto, L.; Lycka, A.; Gilli, G. *J. Am. Chem. Soc.* **2002**, *124*, 13554−13567. (b) Gilli, P.; Bertolasi, V.; Ferretti, V.; Gilli, G. *J. Am. Chem. Soc.* **2000**, *122*, 10405−10417.
(7) *Photochromism: Molecules and Systems. Studies in Organic Chemistry 40*; Durr, H., Bouas-Laurant, H., Eds.; Elsevier: Amsterdam, 1990; Chapter 17 and references therein.
(8) (a) Zimmerman, H. E.; Nesterov, E. E. *J. Am. Chem. Soc.* **2002**, *124*, 2818−2830. (b) Zimmerman, H. E.; Nesterov, E. E. *Acc. Chem. Res.* **2002**, *35*, 77−85. (c) Zimmerman, H. E.; Sebek, P.; Zhu, Z. *J. Am. Chem. Soc.* **1998**, *120*, 8549−8550. (d) Johnnson, B. A.; Kleinman, M. H.; Turro, N. J.; Garcia-Garibay, M. A. *J. Org. Chem.* **2002**, *67*, 6944−6953. (e) Johnson, B. A.; Hu, Y.; Houk, K. N.; Garcia-Garibay, M. A. *J. Am. Chem. Soc.* **2001**, *123*, 6941−6942. (f) Keating, A. E.; Shin, S. H.; Houk, K. N.; Garcia-Garibay, M. A. *J. Am. Chem. Soc.* **1997**, *119*, 1474−1475.
(9) Stoeckenios, W.; Bogomolni, R. A. *Annu. Rev. Biochem.* **1982**, *52*, 587−616.
(10) Choi, T.; Peterfy, K.; Khan, S. I.; Garcia-Garibay, M. A. *J. Am. Chem. Soc.* **1996**, *118*, 12477−12478.
(11) Liebovittch, M.; Olovson, G.; Scheffer, J. R.; Trotter, J. *J. Am. Chem. Soc.* **1997**, *119*, 1462−1463.
(12) Liebovittch, M.; Olovson, G.; Scheffer, J. R.; Trotter, J.; Ramamurthy, V.; Sundarababu, G. *J. Am. Chem. Soc.* **1996**, *118*, 1219−1220.
(13) Amarendra, Kumar, V.; Venkatesan, K. *J. Chem. Soc., Perkin Trans 2* **1991**, 829−835.
(14) (a) Schrel, M.; Haarer, D.; Fischer, J.; Decian, A.; Lehn, J.-M.; Eichen, Y. *J. Phys. Chem.* **1996**, *100*, 16175−16186. (b) Eichen, Y.; Lehn, J.-M.; Scherl, M.; Haarer, D.; Fischer, J.; DeCian, A.; Corval, A.; Trommsdorff, H. P. *Angew. Chem., Int. Ed. Engl.* **1995**, *34*, 2530−2533. (c) Khatib, S.; Botoshansky, M.; Eichen, Y. *Acta Crystallogr.* **1997**, *B53*, 306−316.
(15) (a) Sixl, H.; Warta, R. *Chem. Phys.* **1985**, *94*, 147−155. (b) Ziane, O.; Casalegno, R.; Corval, A. *Chem. Phys.* **1999**, *250*, 199−206. (c) Sousa, J. A.; Loconti, J. D. *Science* **1964**, *146*, 397−398.
(16) (a) Eichen, Y.; Botoshansky, M.; Peskin, U.; Scherl, M.; Haarer, D.; Khatib, S. *J. Am. Chem. Soc.* **1997**, *119*, 7167−7168. (b) Schmidt, A.; Kababya, S.; Appel, M.; Khatib, S.; Botoshansky, M.; Eichen, Y. *J. Am. Chem. Soc.* **1999**, *121*, 11291−11299.
(17) Godsi, O.; Peskin, U.; Kapon, M.; Natan, E.; Eichen, Y. *Chem. Commun.* **2001**, *20*, 2132−2133.
(18) Bodalski, R.; Michalski, J.; Moltkowska, B. *Ann. Soc. Chim. Pol.* **1969**, *43*, 677−681.
(19) See Supporting Information for the complete crystallographic data.
(20) "Collect" data collection software, Nonius B.V., 1998.
(21) (a) Otwinowski, Z.; Minor, W. Processing of X-ray Diffraction Data Collected in Oscillation Mode. *Methods Enzymol.* **1997**, *276*. (b) *Macromolecular Crystallography*; Carter, C. W., Jr., Sweet, R. M., Eds.; Academic Press: New York; Part A, pp 307−326, 1997.
(22) Sheldrick, G. M. *Acta Crystallogr.* **1990**, *A46*, 467−473.
(23) Sheldrick, G. M. *SHELXL97*, Program for the refinement of crystal structures; University of Goettingen, Germany, 1997.
(24) Farrugia, L. J. WinGX V.1.64.05. *J. Appl. Crystallogr.* **1999**, *32*, 837−838 (an integrated system of Windows programs for the solution, refinement, and analysis of single-crystal X-ray diffraction data).

Scheme 1. Ketopyridine (**CH**)−Enolpyridine (**OH**)−Ketoenamine (**NH**) Tautomerization Equilibrium in 1,3-Bis(pyridin-2-yl)propan-2-one, **1**

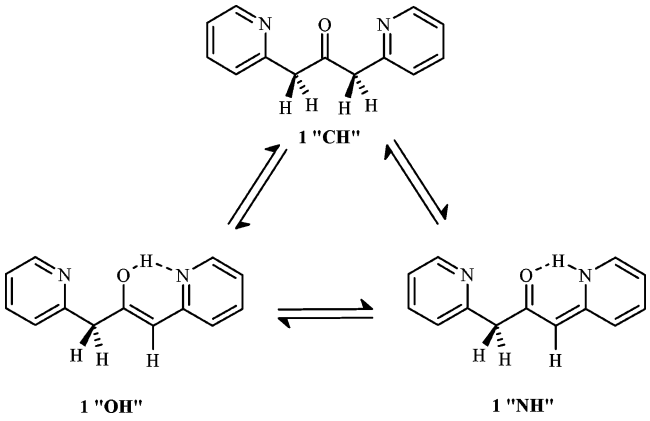

the ketopyridine, **CH**, the enolpyridine, **OH,** and the keto-enamine, **NH**, Scheme 1.

In solutions, such as chloroform and DMSO, two distinct sets of peaks are found in the proton NMR spectrum, attributed to the keto (major) and ene-X (presumably, a rapidly exchanging mixture of ketoenamine and enolpyridine) tautomers, respectively. Assuming a three state model in which the **OH** and **NH** tautomers are energetically degenerate, the energy difference between these tautomers and the **CH** tautomer is given by eq 1

$$\left(\frac{1-\rho_{\mathbf{CH}}}{2\rho_{\mathbf{CH}}}\right)=\exp\left(\frac{-\Delta G}{RT}\right) \qquad (1)$$

where $\rho_{\mathbf{CH}}$ is the measured populations of the **CH** tautomer. The free energy differences between the tautomers at 298 K are 1.2 ± 0.1 and 0.9 ± 0.1 kcal mol^{-1} in DMSO and chloroform, respectively. The separated enol and enamine populations could not be resolved by NMR under any circumstances, probably due to a fast exchange process, attributed to the very low barrier that separates these two species. The keto−ene-X equilibrium is found to be very slow on the NMR time scale because the two distinct sets of peaks do not coalesce even at elevated temperatures in DMSO. Nevertheless, the bands of the acidic protons slowly disappear upon adding D_2O to the solution, evidence for the existence of an equilibrating exchange process.

In the Crystal. Variable-Temperature X-ray Diffractometry. The molecular structure of **1** in the crystal, as derived from diffraction data collected at 293(2) K, is presented in Figure 1.

Crystals of **1** are orthorhombic, space group *Pbcn*, a = 11.1892(4), b = 10.7501(4), c = 17.9978(7) Å, with one molecule in the asymmetric unit. The molecular conformation of the molecules in the crystal is of the ene-X type of tautomers, having an almost planar **N2−C6−C4−O1** dihedral angle,

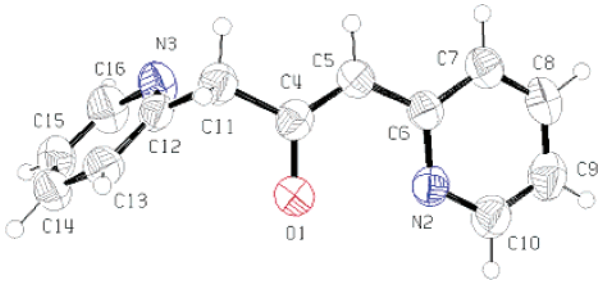

Figure 1. Molecular structure of **1** in the crystal at 293(2) K.

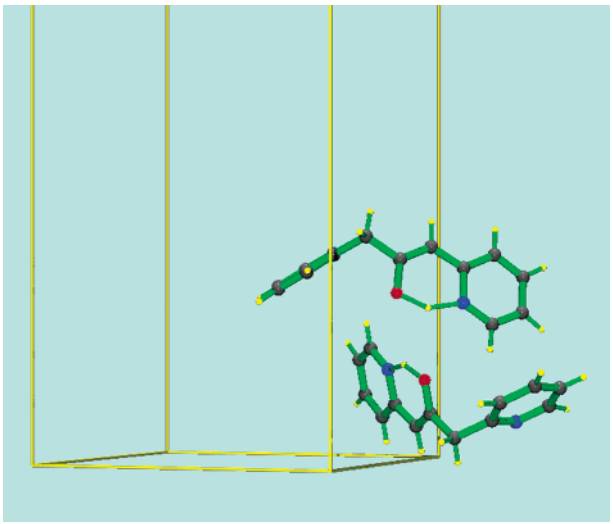

Figure 2. Dimeric structure of molecules of **1** in the crystal lattice.

$\theta_{\mathrm{N2-C6-C4-O1}}$ = 1.1(2)°, where the lone pairs of the basic atoms **O1** and **N2** point to one another, and hosting the acidic proton, $d_{\mathrm{N2-O1}}$ = 2.573(2) Å. The arrangement of the substituents around atom C5 is of a sp^2 character, $\alpha_{\mathrm{C4-C5-C6}}$ = 124.35(2)°.

The molecules of **1** are packed in the crystal in the form of dimers, Figure 2, forming an extended potential well, comprised of four basic atoms; **O1**, **N2**, **O1′**, **N2′**, that host two acidic protons, $d_{\mathrm{O1\cdots N2}}$ = 2.573(2) Å, $d_{\mathrm{O1\cdots O1'}}$ = 3.336(2) Å, $d_{\mathrm{O1\cdots N2'}}$ = 3.351(2) Å, $d_{\mathrm{N2\cdots N2'}}$ = 3.831(2) Å. All other neighboring molecules are situated further away from the reaction site and are assumed to be too far for any significant specific intermolecular interaction that could affect the tautomerization process.

To resolve the exact location and population of the hydrogen atom, H1, electron density Fourier difference maps of a crystal of **1** were recorded at 100, 150, 200, 250, 300, and 330 K. Figure 3 depicts three electron density Fourier difference maps of the crystal of **1** taken at 100, 200, and 300 K.[26]

Two distinct electron density spots are found at the expected positions of the proton in the **OH** and **NH** states. These two spots of high electron density are separated by a saddle of considerably lower electron density, evidence for the presence of a double well potential for the proton with two distinct minima at the **OH** and **NH** states.

At low temperatures, the molecules in a crystal of **1** appear to be mainly in the **OH** form with only a marginal population of the **NH** form. As the temperature increases, the relative

(25) Frisch, M. J.; Trucks, G. W.; Schlegel, H. B.; Scuseria, G. E.; Robb, M. A.; Cheeseman, J. R.; Zakrzewski, V. G.; Montgomery, J. A., Jr.; Stratmann, R. E.; Burant, J. C.; Dapprich, S.; Millam, J. M.; Daniels, A. D.; Kudin, K. N.; Strain, M. C.; Farkas, O.; Tomasi, J.; Barone, V.; Cossi, M.; Cammi, R.; Mennucci, B.; Pomelli, C.; Adamo, C.; Clifford, S.; Ochterski, J.; Petersson, G. A.; Ayala, P. Y.; Cui, Q.; Morokuma, K.; Malick, D. K.; Rabuck, A. D.; Raghavachari, K.; Foresman, J. B.; Cioslowski, J.; Ortiz, J. V.; Stefanov, B. B.; Liu, G.; Liashenko, A.; Piskorz, P.; Komaromi, I.; Gomperts, R.; Martin, R. L.; Fox, D. J.; Keith, T.; Al-Laham, M. A.; Peng, C. Y.; Nanayakkara, A.; Gonzalez, C.; Challacombe, M.; Gill, P. M. W.; Johnson, B. G.; Chen, W.; Wong, M. W.; Andres, J. L.; Head-Gordon, M.; Replogle, E. S.; Pople, J. A. *Gaussian 98*, revision A.11.3; Gaussian, Inc.: Pittsburgh, PA, 1998.

(26) A detailed description of the experiment is presented in the Experimental Section. See the Supporting Information for the complete temperature-dependent crystallographic data.

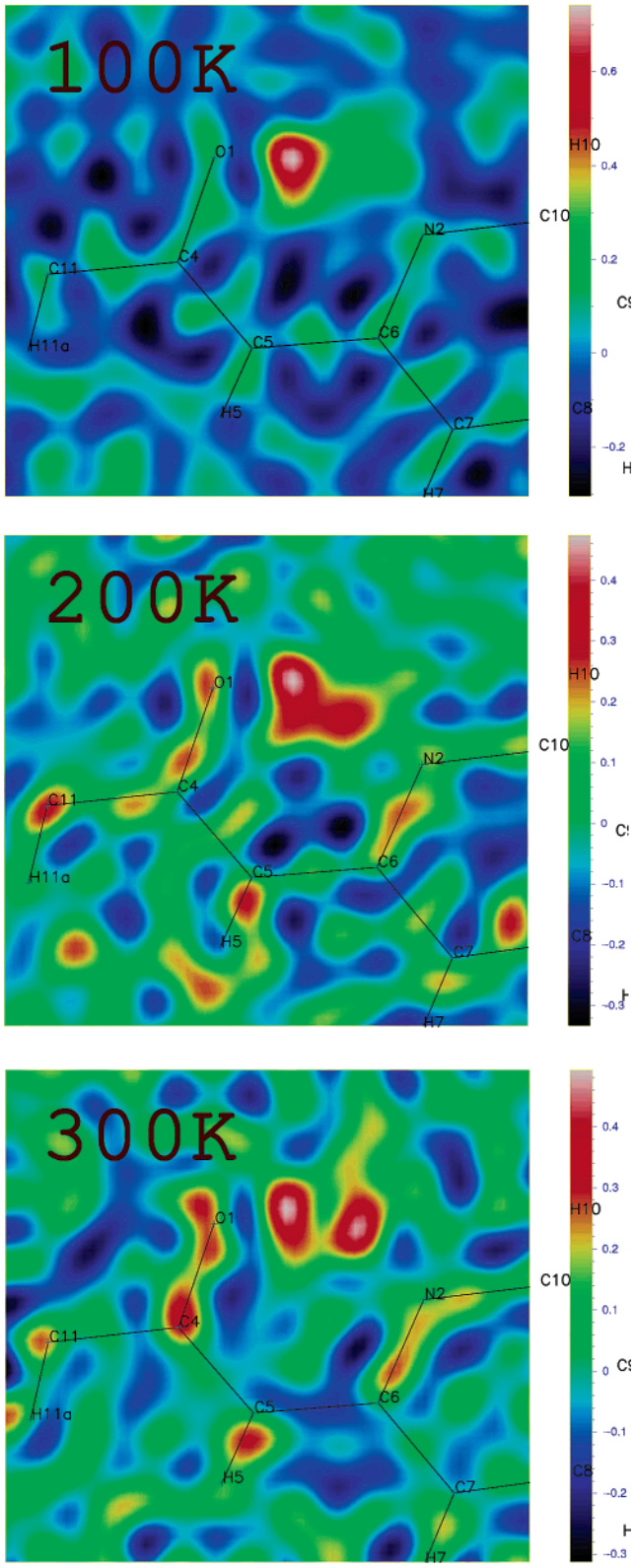

Figure 3. Electron density Fourier difference maps at 100, 200, and 300 K.

population of the **NH** form increases, with a clear tendency toward equal population at elevated temperatures. A plot of the relative population of the **OH** and **NH** tautomeric states as a function of the temperature is depicted in Figure 4. In contrast to the **OH** and **NH** tautomers, the keto, **CH**, tautomer that is

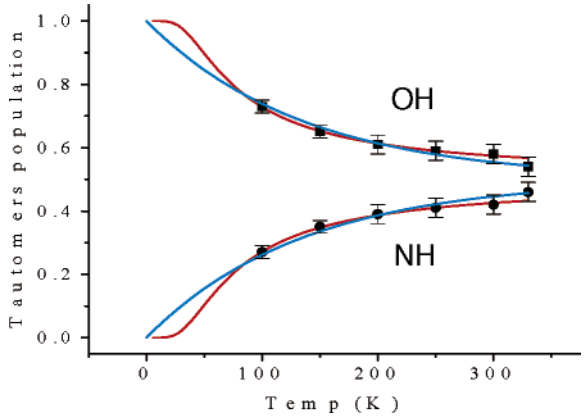

Figure 4. Relative population of the **OH** and **NH** tautomers as measured by X-ray diffraction. The blue and red lines correspond to the best fit to models of two and four level systems, respectively.

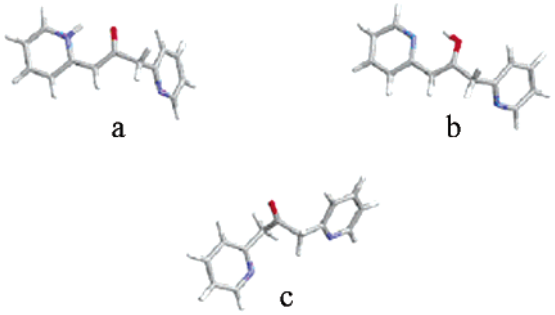

Figure 5. Geometries of the energy-minimized gas-phase tautomers of **1** (MP2/6-31G**): (a) **NH**, (b) **OH**, and (c) **CH**.

Table 1. Relative Energy (kcal mol^{-1}) of the Lowest Energy Conformation of the Different Tautomers in the Gas Phase[a,b]

	HF/6-31G**		MP2/6-31G**		
tautomer	ΔH	d_{N2-O1}	ΔH	d_{N2-O1}	$N_2-C_6-C_4-O_1$
CH	0.00		0.00		−141.5
OH	3.54	2.697	0.98	2.622	0.35
NH	8.39	2.656	6.81	2.531	−0.26

[a] In the crystal at 293 K, d_{N2-O1} = 2.573(2) Å. [b] Distances are in angstroms, and angles are in degrees.

found to be the most stable in solutions was undetectable at all temperatures in the crystal.[27]

Electronic Energy Calculations. To obtain a simple and traceable model for the system, the electronic energy was calculated for the three major tautomers of **1** in the gas phase within the HF/6-31G** and MP2/6-31G** approximations.[28] Figure 5 depicts the geometries of the energy-minimized gas-phase structures of the **CH**, **NH**, and **OH** tautomers, according to the MP2/6-31G** approximation.

Table 1 depicts the relative energy of the different tautomers as well as some important intramolecular parameters. The two approximations suggest a similar order of stability and energy differences between the three tautomers as well as similar optimized structures.

As seen in Table 1, electronic energy calculations predict that the keto **CH** form of **1** is the most stable tautomer in the gas

(27) Crystal data as well as complementary DSC measurements exclude any first-order phase transition throughout the experiment temperature regime. See the Supporting Information for DSC.
(28) Zero-point energy corrections are included in all values of HF calculations, while all values of MP2 were not corrected for zero-point energy due to computer size limitations.

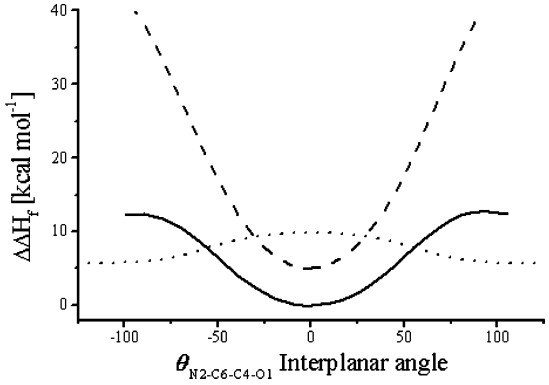

Figure 6. Energy profile of the different tautomers as a function of the **N2−C6−C5−C4** dihedral angle (—) **OH**, (− −) **NH**, and (···) **CH**.

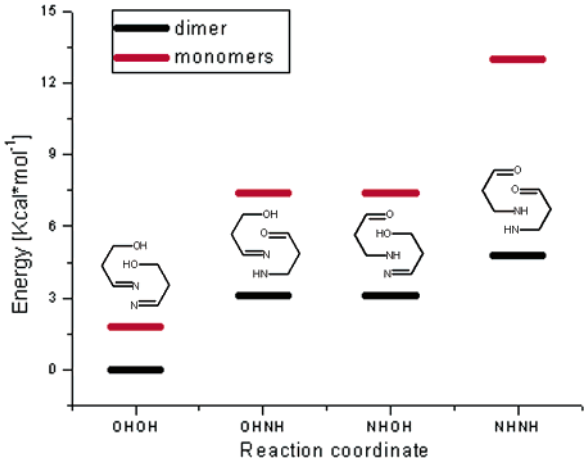

Figure 7. Relative energy of the **OH−OH**, **OH−NH**, and **NH−NH** dimeric states calculated within the HF/6-31G** approximation.

phase, that the **OH** form is somewhat higher in energy, while the **NH** form is considerably higher in energy and is not expected to be detectable at any reasonable temperature. This stability order is consistent with the RAHB approach that predicts increased stability of the **OH** tautomer due to increased conjugation and hydrogen bonding. The **NH** tautomer involves the perturbation of the aromaticity of the pyridine ring and therefore is expected to be high in energy.

The electronic energy profiles of the different tautomeric forms of **1** around its crystallographic conformation were explored by using a model of a constrained single molecule in which four of its dihedral angles, **N3−C12−C11−C4**, **C12−C11−C4−O1**, **N2−C6−C5−C4**, and **C6−C5−C4−O1**, were fixed to their crystallographic values. Because the major difference between the tautomers is expected to originate from the differences in the dihedral angle **N2−C6−C5−C4**, this angle was scanned between +100° and −100°. Figure 6 presents a graph of the energy (calculated using the HF/6-31G** approximation) of each tautomer as a function of the dihedral angle **N2−C6−C5−C4**.

The calculations show that when the fixed dihedral angle **N2−C6−C5−C4** corresponds to its crystallographic value, the two ene-X tautomers (the enolpyridine, **OH**, and the ketoenamine, **NH**) are close to their energy minima while the ketopyridine, **CH**, tautomer appears to be in a maximum point along the energy profile. This calculated difference in the stability of the different tautomers is consistent with the experimental data and rationalizes the absence of the ketopyridine, **CH**, tautomer from the crystal at all experimental conditions. The calculated energy difference between the constrained isolated **OH** and **NH** tautomers having their four dihedral angles fixed to their crystallographic coordinates is found to be as high as $\Delta H_{(\mathbf{OH})-(\mathbf{NH})} = 5.39$ and 6.44 kcal mol^{-1} (using HF/6-31G** and MP2/6-31G**, respectively).

At these energy differences, the higher energy tautomer **NH** is not expected to be significantly populated throughout the entire temperature range of the experiments. Nevertheless, crystallographic measurements on the system clearly show a nonnegligible population of the **NH** tautomer, suggesting a significantly smaller energy difference between the **OH** and **NH** tautomers.

In contrast to the situation in the gas phase, the molecules of **1** appear in the crystal in the form of dimers in which one molecule is dimerized with a second molecule related by the $-x, y, -z + {}^1/_2$ symmetry operation. The dimeric arrangement of **1** in the crystal localizes two additional basic groups and a proton within close proximity to the enol−enamine reaction site. The presence of a neighboring molecule with two basic groups that are close to the tautomerization site are expected to have an effect on the **OH** ⇄ **NH** equilibrium.

To estimate the effect of the specific interactions within the reaction site in the crystal, the nearest neighbor of the reacting molecule was added to the model. The effect of dimerization of **1** on the enolpyridine−ketoenamine thermodynamic equilibrium was calculated by comparing the energy of the different tautomeric combinations: (**OH−OH**), two degenerate states (**OH−NH**) and (**NH−OH**), and (**NH−NH**). The dimeric form found in the crystal was modeled in the calculation by placing the molecules at the crystallographic coordinates and fixing all dihedral angles, except the ones of the tautomering protons. Additionally, the intermolecular distances and angles between atoms of the two nonreacting pyridine rings, **C16−C16′**, **C13−C14′**, **C14−C13′**, **C16−C16′−N3**, and **C13−C14′−C13′**, were fixed. Figure 7 depicts the relative energies of the (**OH−OH**), (**OH−NH**), and (**NH−NH**) dimeric states, calculated within the HF/6-31G** approximation. The energy diagram of the two separated monomers (taken at the same intramolecular geometrical constraints, but put at an intermolecular distance of 30 Å) is also provided for comparison. As can be seen, the assembly of two molecules of **1** into the dimeric structure found in the crystal has a dramatic effect on the energy diagram of the different tautomers. This implies that the minimal structure to be considered in the crystal lattice is the dimer and that the system is of four distinct energy levels of which two, (**OH−NH**) and (**NH−OH**), are degenerate.

All of the tautomeric states are stabilized in the dimer with respect to the separated monomers. However, while the (**OH−OH**) dimeric state is only slightly stabilized (1.62 kcal mol^{-1}) with respect to its monomers, the dimeric (**NH−NH**) state is significantly stabilized (7.91 kcal mol^{-1}) and the two degenerate (**OH−NH**) and (**NH−OH**) states are moderately stabilized (4.06 kcal mol^{-1}). The different stabilization of different tautomeric states influences the energy gaps between them. In the dimer, the first excited tautomerization states (**OH−NH**) and (**NH−OH**) are only 2.95 kcal mol^{-1} higher than the (**OH−OH**) state, while the (**NH−NH**) state is only 1.54 kcal mol^{-1} higher than the later ones. The model calculations suggest therefore an

overall effect of reducing the energy gaps between the different tautomeric states due to the intermolecular interactions in the dimer.

While the approximated electronic energy calculations should not be expected to be quantitatively comparable to the experimental data, they suggest a reasonable platform for interpreting the measured temperature dependence of the hydrogen position in the crystal, based on a four-state model. The experimental data, obtained from the crystallographic experiments, were fitted to a model based on a Boltzmann temperature-dependent population of the different tautomers. Assuming that the difference in the free energy between the tautomers is primarily due to their electronic structure and to high-frequency (**OH** or **NH**) modes, the temperature dependence of the different ΔG values below was neglected.[29] The relative electron densities of the labile proton at the **OH** and **NH** positions were used for extracting the energy levels of the system, using eq 2, where $\rho_{\mathbf{OH}}$ and $\rho_{\mathbf{NH}}$ are the measured relative populations of the **OH** and **NH** tautomers, respectively.

$$\frac{\rho_{\mathbf{NH}}}{\rho_{\mathbf{OH}}} = \frac{\exp\left(\frac{-\Delta G_{(\mathbf{OH-OH})-(\mathbf{OH-NH})}}{RT}\right) + \exp\left(\frac{-\Delta G_{(\mathbf{OH-OH})-(\mathbf{OH-NH})} - \Delta G_{(\mathbf{OH-NH})-(\mathbf{NH-NH})}}{RT}\right)}{1 + \exp\left(\frac{-\Delta G_{(\mathbf{OH-OH})-(\mathbf{OH-NH})}}{RT}\right)} \quad (2)$$

The red line in Figure 4 represents the best fit of the four energy state model to the experimental data, assuming $\Delta G_{(\mathbf{OH-OH})-(\mathbf{OH-NH})} = 120 \pm 10$ cal mol^{-1} and $\Delta G_{(\mathbf{OH-NH})-(\mathbf{NH-NH})} = 50 \pm 10$ cal mol^{-1}. If the effect of dimerization is ignored and only two states are considered in the energy level diagram, then the **OH** to **NH** energy difference is calculated to be $\Delta G_{(\mathbf{OH})-(\mathbf{NH})} = 178 \pm 3$ cal mol^{-1}. As one can see, the two models produce a reasonable fit to the experimental data. Nevertheless, the calculations suggest that the intermolecular coupling between the monomers in the crystal is significant and the dimer model is likely to be more appropriate for this system.

An important difference between the four-level model (dimer) and the two-level model (monomer) relates to the hydrogen vibrations expected from the two systems. While the vibrational normal modes of the isolated monomers include a **O−H** vibration in the enolpyridine form, and an **N−H** vibration in the ketoenamine form, the normal-mode analysis of the constrained dimer model reveals modes in which the motions of two protons, associated with the two molecules, are coupled. These intermolecular hydrogen modes are illustrated in Figures 8 and 9.[30] The emergence of such coupled vibrations is a direct indication for intermolecular coupling. The calculated frequency differences between the monomers and the dimers are noticeable (a few cm^{-1}) and reflect the magnitude of the intermolecular coupling in the crystal. Moreover, in the cases of symmetric (**OH−OH**) or (**NH−NH**) dimers, where the hydrogen frequencies in the two monomers are identical, the two hydrogen modes in the dimer involve a nearly symmetric and a nearly antisymmetric concerted motion of the two hydrogen atoms (Figures 9 and 8, respectively) The two calculated frequencies differ by a few wavenumbers and have different IR and Raman activities due to their different symmetry. One vibration is dominant in the IR spectrum, while the other dominates the Raman spectrum. A measurement of these vibrations, which are unique to the dimer, can thus provide conclusive evidence for the significance and for the intensity of the intermolecular coupling within the crystal. Unfortunately, the performance of such an experiment is beyond our experimental capabilities because the crystal is strongly luminescent. We therefore limit our discussion to a prediction that these bands should be present in the infrared spectra.

(29) See the mathematical appendix part C in the Supporting Information.
(30) See the mathematical appendix part D in the Supporting Information.

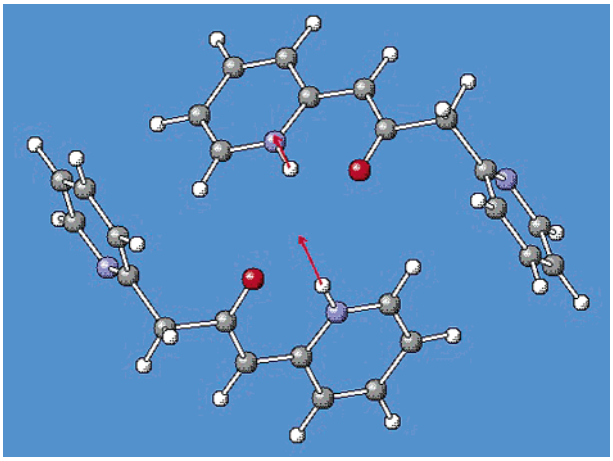

Figure 8. **NH−NH** dimer model. The arrows indicate an anti-symmetric concerted motion of the two hydrogen atoms, indicative of intermolecular coupling.

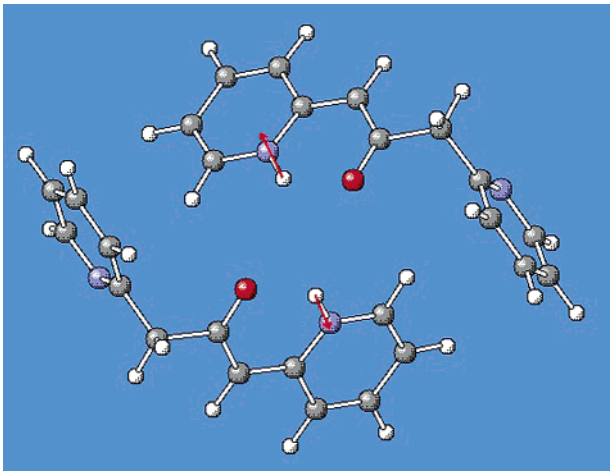

Figure 9. **NH−NH** dimer model. The arrows indicate a symmetric concerted motion of the two hydrogen atoms, indicative of intermolecular coupling.

Conclusions

The enolpyridine, **OH**−ketoenamine, **NH** equilibrium was studied in single crystals of 1,3-bis(pyridin-2-yl)propan-2-one using temperature-dependent single-crystal X-ray diffraction and electronic energy calculations. The temperature-dependent relative population of the different tautomers was determined, showing a strong temperature dependence of the population of the different tautomers. Electronic energy calculations for the molecule in the isolated gas-phase state and in monomeric and dimeric states, which were constrained to the crystallographic molecular geometry, revealed the important effect of dimeriza-

tion of the reacting molecules on the tautomerization potential energy surface and on the keto−enol−enamine equilibrium.

Several main dimeric tautomer states were identified for the supramolecular dimer, of which four are probably accessible in the crystalline state, and can account for the measured temperature dependence of the hydrogen position in the crystal. The theoretical model suggested the appearance of concerted hydrogen motions which are unique to the dimer and which can be used to quantify the effect of the supramolecular interaction on the hydrogen population in the crystal. Experimental work in this direction is in progress.

Acknowledgment. This research was supported by the Israel Science Foundation (ISF) and the United States−Israel Binational Science Foundation (BSF).

Supporting Information Available: Additional crystallographic data, CIF files, and electron density Fourier difference maps of the temperature-dependent crystallographic data, DSC, tables of all of the energies of the different calculations and their output files, and mathematical appendices. This material is available free of charge via the Internet at http://pubs.acs.org.

JA046311H